

Effect of the LPSO volume fraction on the microstructure and mechanical properties of Mg–Y_{2x}–Zn_x alloys

E. Oñorbe · G. Garcés · P. Pérez · P. Adeva

Received: 25 May 2011 / Accepted: 24 August 2011 / Published online: 7 September 2011
© Springer Science+Business Media, LLC 2011

Abstract The influence of the volume fraction of long-period stacking ordered structure (LPSO) on the microstructure and mechanical properties in three extruded Mg_{100-3x}Y_{2x}Zn_x alloys ($x = 0.5, 1$ and 1.5 at.%) has been studied. Two structures of LPSO phase coexist in these extruded alloys, 18R and 14H. The 18R structure transforms to 14H structure gradually in the course of the extrusion process. For the three alloys, the grain size in the vicinity of LPSO phase particles is refined because of a particle-stimulated nucleation (PSN) mechanism. The reinforcing effect of the LPSO phase is active up to 523 K. Above this temperature, grain size effect becomes important. Accordingly, MgY₁Zn_{0.5} extruded alloy shows the Highest mechanical strength for temperatures greater than 523 K.

Introduction

The use of magnesium alloys as structural materials has been motivated because of increasing social awareness of the need of energy saving and material recyclability. However, their industrial applications have been limited because conventional magnesium alloys show poor corrosion resistance, poor ductility and low mechanical and creep resistance. All these disadvantages limit their use for structural applications [1].

The addition of yttrium and/or rare-earth elements to magnesium improves its mechanical strength at room and high temperatures because of the fine dispersion of intermetallic second-phases. In the last decades, different systems based on magnesium–yttrium/rare earth elements have been developed, such as AE, WE and EZ alloys. These systems have shown a higher creep resistance than other commercial magnesium alloys [2].

The Mg–Zn–Y system seems particularly promising because it exhibits a higher mechanical performance with respect to commercial alloys based on the binary Mg–Zn system. The addition of yttrium promotes the formation of intermetallic phases whose stability is retained up to high temperature [3]. Depending on the atomic Zn/Y ratio, different ternary phases can be formed: I-phase Mg₃YZn₆ (icosahedral), W-phase Mg₃Y₃Zn₂ (fcc), H-phase MgYZn₃ (hexagonal) or Z-phase Mg₁₂YZn (hexagonal) [3–7].

Inoue et al. [7] developed a Mg₉₇Y₂Zn₁ (at.%) alloy by warm extrusion of rapid solidified powders at 573 K that exhibited a high yield strength, about 610 MPa, with 5% of elongation at room temperature. The high strength of this alloy arises from their fine grain size and the presence of a long-period stacking ordered structure (LPSO). This phase forms when the atomic Y/Zn ratio in the Mg–Zn–Y system is 2:1. The LPSO phase consists of a solid solution of Y and Zn in a magnesium matrix where these atoms are placed periodically in the magnesium basal planes forming an ordered structure [8]. Different LPSO structures have been reported in the bibliography, i.e., 6H, 10H, 14H, 18R and 24R [9–11] depending of the thermal history of the material. The 18R structure, which is the most commonly observed, presents the same structure of the X-Mg₁₂YZn phase reported by Luo et al. [12]. Recently, Zhu et al. [13] have concluded that 6H-stacking sequence is a segment of the stacking in the 18R unit cell.

E. Oñorbe (✉) · G. Garcés · P. Pérez · P. Adeva
Department of Physical Metallurgy, Nacional Center for Metallurgical Research, CENIM-CSIC. Av. Gregorio del Amo, 8, 28040 Madrid, Spain
e-mail: elvionorbe@gmail.com

Fig. 1 Microstructures of the alloys in the as-cast condition. **a** $\text{MgY}_1\text{Zn}_{0.5}$, **b** MgY_1Zn_2 and **c** $\text{MgY}_3\text{Zn}_{1.5}$

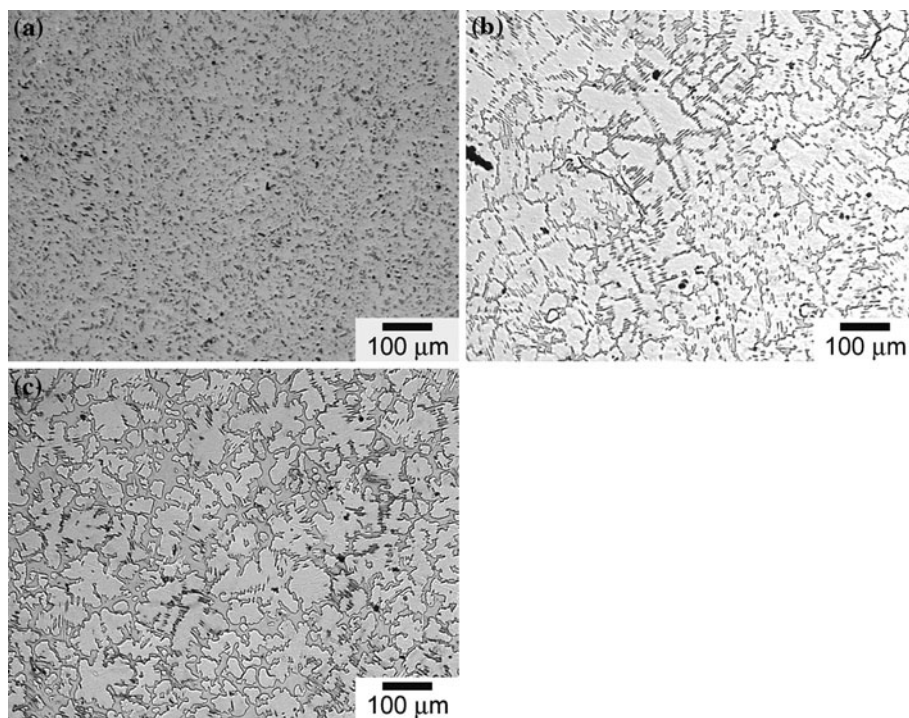
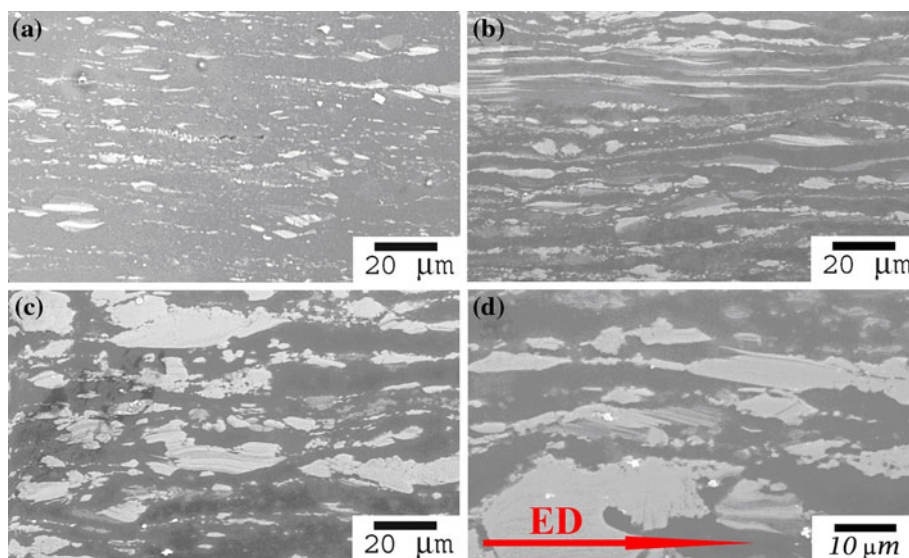


Fig. 2 Microstructures of the as-extruded alloys **a** $\text{MgY}_1\text{Zn}_{0.5}$, **b** MgY_2Zn_1 and **c** $\text{MgY}_3\text{Zn}_{1.5}$. **d** Detail of LPSO phase of **c**



Mechanical properties of the Mg–RE–Zn alloys containing the LPSO phase are greatly superior than those reported for quasicrystalline-containing alloys [14]. Different authors have proposed models about the strengthening mechanisms in magnesium alloys with LPSO phase. Matsuda et al. [15] have reported that $\langle c + a \rangle$ dislocations were observed in Mg grains with LPSO precipitates, instead of $\langle a \rangle$ dislocations on the basal plane. The result implies that the formation of a LPSO phase increases the critical resolved shear stress of the basal slip, activating non-basal slip in the Mg matrix. Ab initio calculations

within the framework of density functional theory have validated this theory [16]. Magnesium alloys can also deform by twinning. Matsuda et al. [17] have reported that the $\{10\bar{1}2\}$ deformation twin is deflected or arrested in the region where the LPSO phase develops with high density, i.e. the twin propagates along the edge of bundled LPSO phase and the twin front arrests parallel to the basal plane of LPSO phase.

Hagihara et al. [18] studied the plastic behaviour of the 18R LPSO phase, showing a high plastic anisotropy. When the stress was applied parallel to the (0001) plane, i.e. the

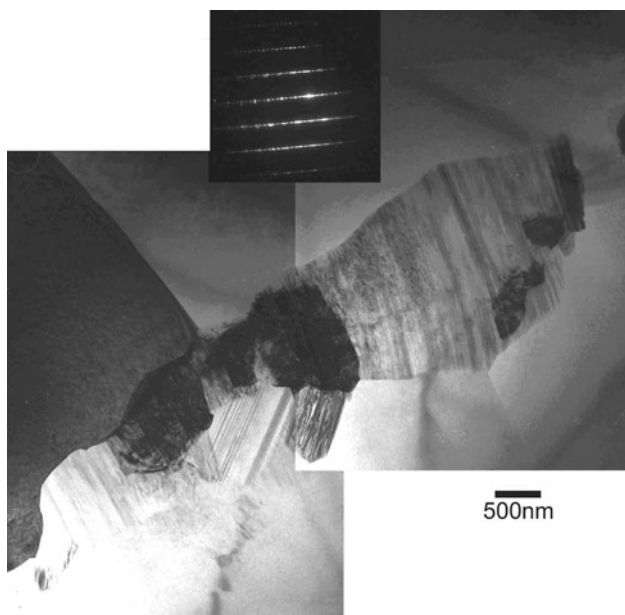


Fig. 3 Bright field image of extruded MgY₂Zn₁ alloy showing a detail of LPSO phase and SAED taken from the LPSO phase. [11 $\bar{2}$ 0] zone axis



Fig. 4 Bright field image of extruded MgY₃Zn_{1.5} showing the LPSO phase delaminated

Schmid factor for basal slip was negligible, deformation kinks were initiated in the LPSO phase, accommodating the strain up to some extent. Kink deformation is an

essential mechanism to generate homogeneous strain in crystals, contributing to enhance ductility of the material. During kinking process, dislocations are accumulated inside the LPSO phase, inducing a considerable increase in hardness [19].

The purpose of this work is to study the effect of volume fraction of LPSO phases on the microstructure and mechanical properties of Mg–Y–Zn alloys. Therefore, three extruded Mg–Y–Zn alloys of a constant Y/Zn atomic ratio of 2:1 were prepared.

Experimental procedure

Alloys, with nominal composition of Mg_{98.5} Y_{1.0}Zn_{0.5} (at.%), Mg_{97.0} Y_{2.0}Zn_{1.0} (at.%) and Mg_{95.5} Y_{3.0}Zn_{1.5} (at.%), were prepared by melting high-purity elements Mg and Zn and a Mg-22%Y master alloy in an electric resistance furnace. The alloys were cast in a cylindrical steel mould (42-mm diameter). Then, cast rods were extruded at 723 K, employing an extrusion ratio of 18:1. Prior the extrusion stage, the cast rod was maintained 20 min at 723 K.

Microstructural characterization of the alloys was carried out by X-ray diffraction (XRD) and optical, scanning and transmission electron microscopy. XRD pattern was performed using a SIEMENS TM Kristalloflex D5000 diffractometer equipped with a close Eulerian cradle. The X-radiation used was β -filtered Cu-K α . The diffraction pattern was measured in polished surfaces perpendicular to the extrusion direction.

Metallographic preparation for optical and SEM observations consisted of mechanical polishing and etching in a mixture of 5 ml of acetic acid, 20 ml of water and 25 ml of a solution of picric acid in methanol. Specimens for TEM observations were prepared by electrolytic polishing using the reactive mixture of 25% nitric acid and 75% methanol at 253 K and 20 V. Then, ion milling at liquid nitrogen temperature was used to remove the fine oxide film formed on the surface during electrolytic polishing. Grain size and volume fraction of phases were estimated by image analysis technique using at least ten areas for each alloy.

Microhardness measurements were performed with a load of 500 g during 15 s. Young’s modulus and hardness of the matrix and LPSO phase were also determined with a Micro Materials NanoTest 600 equipment. Indentations with a Berkovich type indenter were performed normal to the polished cross-sections by using a maximum load of 50 mN. The hardness, *H*, and the Young’s modulus, *E*, were evaluated from the load and the depth indentation curves taking into account the Oliver and Pharr method [20].

Mechanical properties of extruded alloys were determined by tensile tests. Cylindrical samples (head diameter 6 mm, curvature radius 3 mm, gauge diameter 3 mm and

Fig. 5 Bright field image and SAED of the MgY_2Zn_1 extruded alloy showing isolated LPSO lamella precipitated within the magnesium matrix. $[11\bar{2}0]$ zone axis

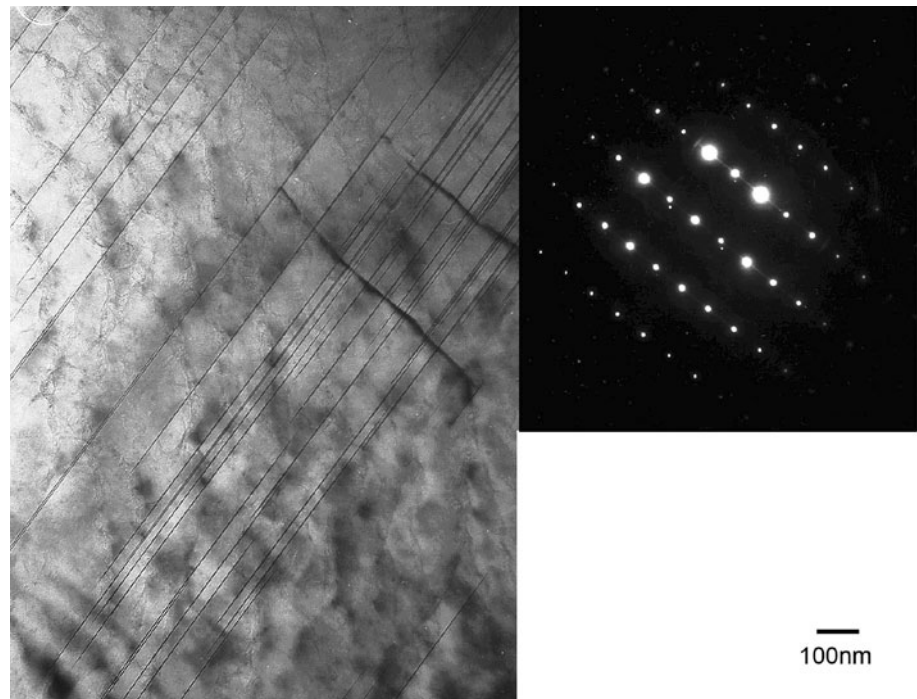


Table 1 Volume fraction of LPSO phase and Vickers Hardness values for the three alloys

Alloy	%LPSO	HV
$\text{MgY}_3\text{Zn}_{1.5}$	35	84.7 ± 0.6
MgY_2Zn_1	21	82.5 ± 0.7
$\text{MgY}_1\text{Zn}_{0.5}$	9	65.4 ± 1.1

gauge length 10 mm) were machined with their long direction parallel to the extrusion direction. Tensile tests from room temperature to 673 K were performed in a universal tensile machine with constant cross-head speed at an initial strain rate of 10^{-4} s^{-1} .

Results and discussion

Microstructure

Figure 1a–c shows metallographic images of the alloys in the as-cast condition. Two phases are well resolved, the magnesium matrix and a secondary phase distributed in the interdendritic region, with lamellar morphology. After extrusion at 723 K, the lamellar phase was broken, elongated and oriented along the extrusion direction as shown in Fig. 2. The LPSO phase was homogeneously distributed throughout the magnesium matrix, being located at the boundaries of the original magnesium dendrites.

The TEM image of Fig. 3 shows the microstructure as well as a detail of the LPSO phase for the extruded

$\text{Mg}_{97}\text{Y}_2\text{Zn}_1$ (at.%) alloy. During extrusion, the LPSO phase is hardly deformed and they fragment into smaller particles. It is interesting to note the formation of kinks bands within the coarser LPSO. This fact has also been reported during compression at high temperature in the $\text{Mg}_{97}\text{Y}_2\text{Zn}_1$ (at.%) alloy [19]. Moreover, this phase appears delaminated along the basal planes in the case of the alloy with the higher volume fraction of the LPSO phase, i.e. $\text{Mg}_{96.5}\text{Y}_3\text{Zn}_{1.5}$ (at.%) alloy, as shown Fig. 4. It was also observed the presence of isolated thin plates within the magnesium matrix grains that must be formed during the extrusion process (Fig 5). These lamellae are fully coherent with magnesium matrix as shown in the strike observed in SADP along $[0002]$ direction.

The volume fraction of LPSO phase varies depending on the alloy composition. As expected, the volume fraction of LPSO phase increases with increasing Y and Zn contents (Table 1) from 9% for the less alloyed material to 35% for the highest. The grain structure along the extrusion direction for the three alloys is shown in Fig. 6. Grain size is inhomogeneous in these alloys, being finer in the vicinities of the LPSO phase (Fig. 6d). Figure 7 shows the histogram of the grain size distribution for the three alloys. The fine-grained areas are usually close to the broken LPSO phase as has been commented above, being the grain size between 1 and 5 μm . The grain size of coarse-grained areas ranges between 8 and 30 μm . The grain size seems to follow a LogNormal distribution in the three cases, although the volume fraction of fine grain areas increases as the volume fraction of the LPSO phase increases.

Fig. 6 Grain structure along extrusion direction for **a** $MgY_1Zn_{0.5}$, **b** MgY_2Zn_1 and **c** $MgY_3Zn_{1.5}$. **d** Detail of grain structure in the vicinity of LPSO phase

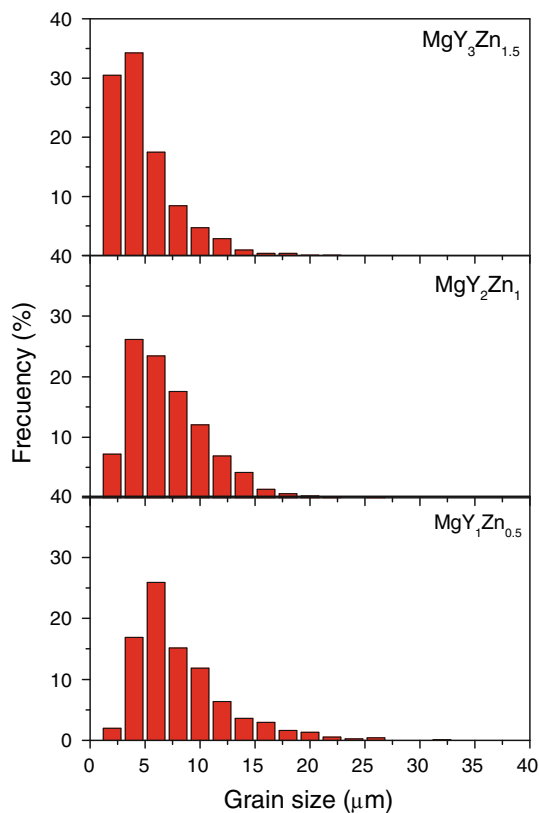
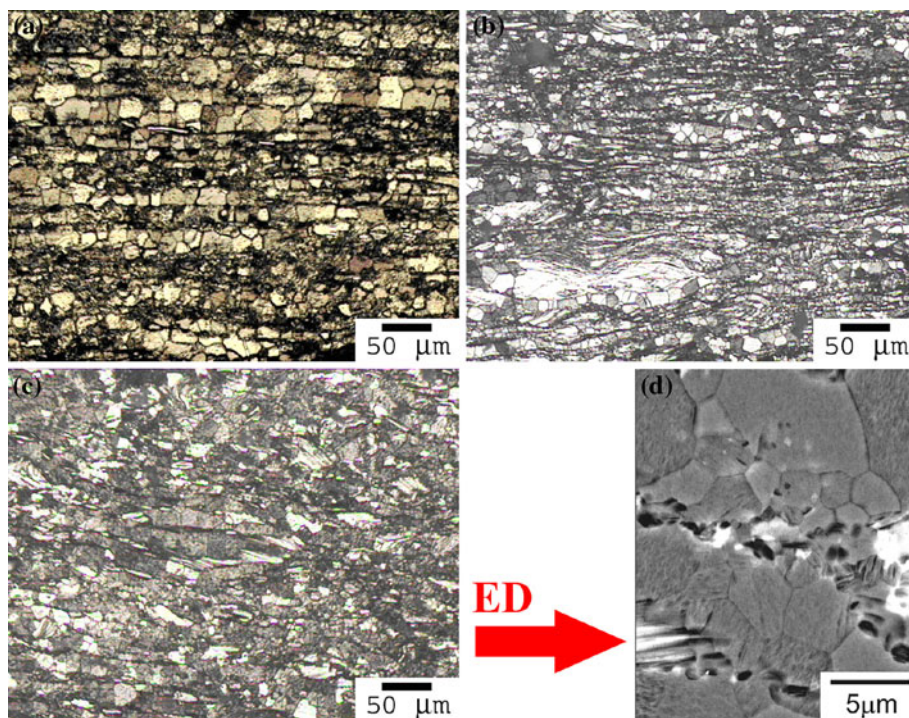


Fig. 7 Histogram of the grain size distribution for the three alloys

Grain size refinement in the vicinity of the LPSO phase is attributed to the fact that recrystallization of the magnesium matrix is induced during extrusion through the

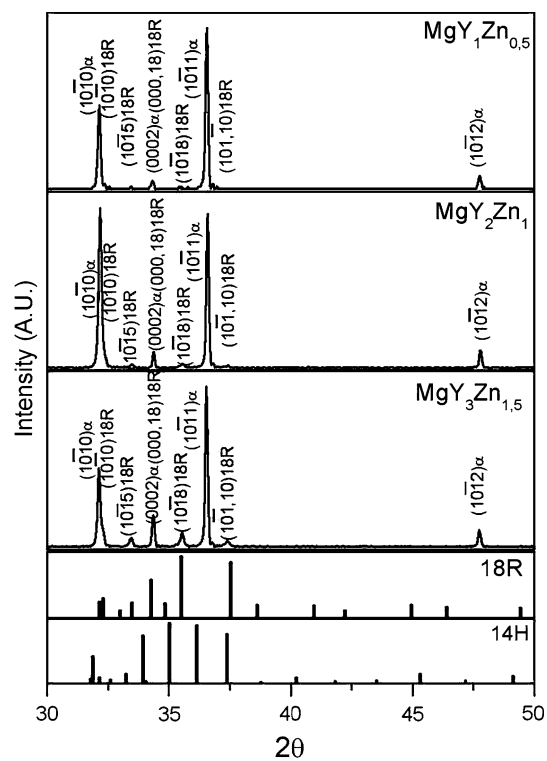
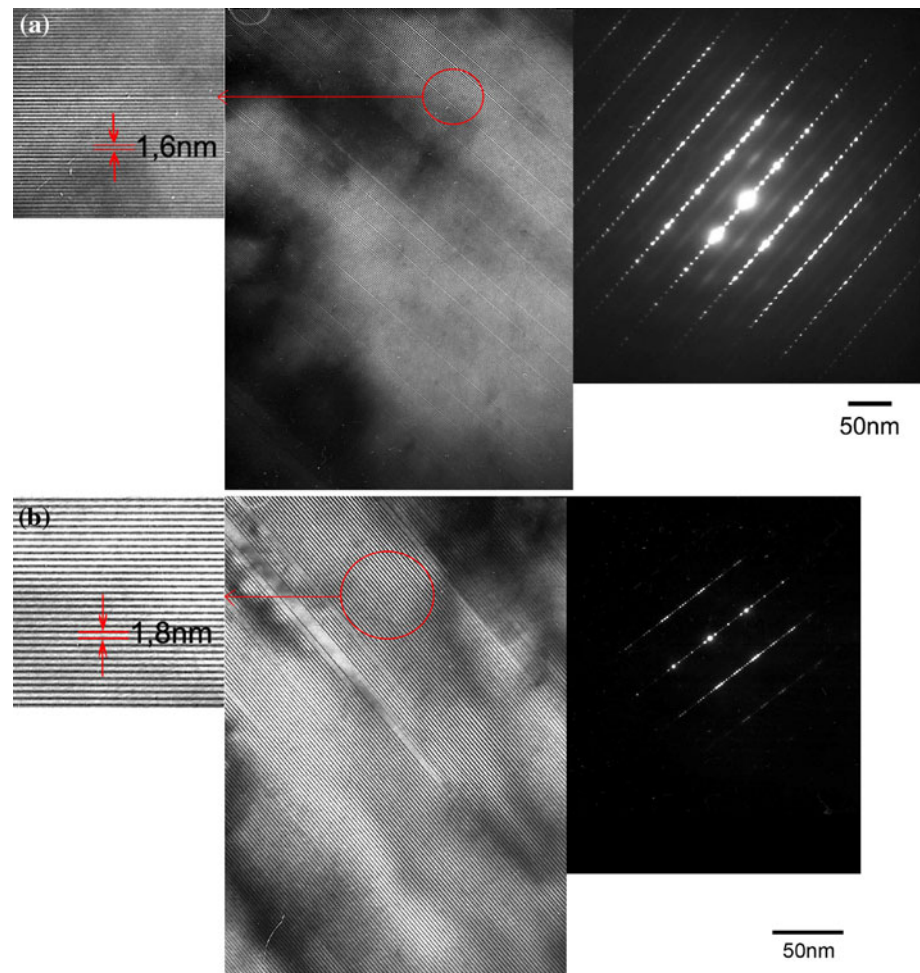


Fig. 8 XRD pattern for the three alloys. The simulated patterns for 18R and 14H structures using CaRine Crystallography 3.1 [24] are also included in the bottom of the figure

mechanism known as particle-stimulated nucleation (PSN) at the LPSO–Mg interfaces [21, 22]. Furthermore, the broken LPSO phase particles block further growth of

Fig. 9 Bright field images of the LPSO phase and SAED in the extruded MgY_2Zn_1 alloy. $[11\bar{2}0]$ zone axis. **a** 18R structure and **b** 14H structure



recrystallised grains. The PSN mechanism involves a rapid sub-boundary migration in the deformation zone that was developed during extrusion around large hard particles with a diameter $>1 \mu\text{m}$ (Fig. 2 shows that LPSO phase is coarser than $1 \mu\text{m}$). The accumulation of misorientation by the rapid sub-boundary migration has to be enough to generate high-angle grain boundaries (HAGBs).

The presence of the 18R LPSO structure was confirmed by XRD measurements in the three alloys, as shown in Fig. 8. This result is in agreement with XRD diffraction pattern in cast $\text{Mg}_{97}\text{Y}_2\text{Zn}_1$ (at.%) alloy given by Yamasaki et al. [23]. The intensity of 18R LPSO phase peaks increases as the volume fraction of this phase increases. It is interesting to point out that the more intense diffracted peak in the $\text{Mg}_{100-3x}\text{Y}_{2x}\text{Zn}_x$ alloys corresponds to the $\{10\bar{1}0\}$ plane. This fact indicates that all alloys develop a typical extrusion texture with the basal planes parallel to the extrusion direction, in agreement with the data recently reported by Hagihara et al. [25]. The existence of 14H LPSO structure cannot be unambiguously confirmed in XRD patterns, because diffraction peaks attributed to this phase overlap with those of Mg, and the difference in the

diffraction angle between Mg and 14H LPSO phase is negligible. Nevertheless, previous studies have pointed out that 18R LPSO structure transformed gradually into the 14H LPSO structure when the alloy is annealed greater than 623 K [9, 26–28]; therefore, the existence of this phase in the present alloys cannot be excluded.

TEM studies were carried out to determine the crystallographic structure of the LPSO phase. It is possible to distinguish easily these structures through the selected area electron diffraction pattern (SAED) as well as measuring the fringes spacing in the $(0002)_\alpha$ direction formed when the $g(0002)$ are excited. Figure 9 shows the 18R and 14H LPSO structures observed in the extruded alloys. On one hand, Fig. 9a shows the 18R structure with a fringe spacing of about 1.6 nm measured in $\langle 11\bar{2}0 \rangle_\alpha$ zone axis. The SAED pattern shows weak streaks along the direction of $g(0001)_\alpha$ and through $\pm 1/2\{1\bar{1}00\}_\alpha$ positions are visible in the SAED pattern. Zhu et al. [13] indicated that the presence of these weak streaks provide important information on the ordered arrangement of Y and Zn atoms in the 18R structure. They tried to demonstrate that such reflections would not have existed if Y and Zn atoms were disordered arrangement in the unit cell. On the

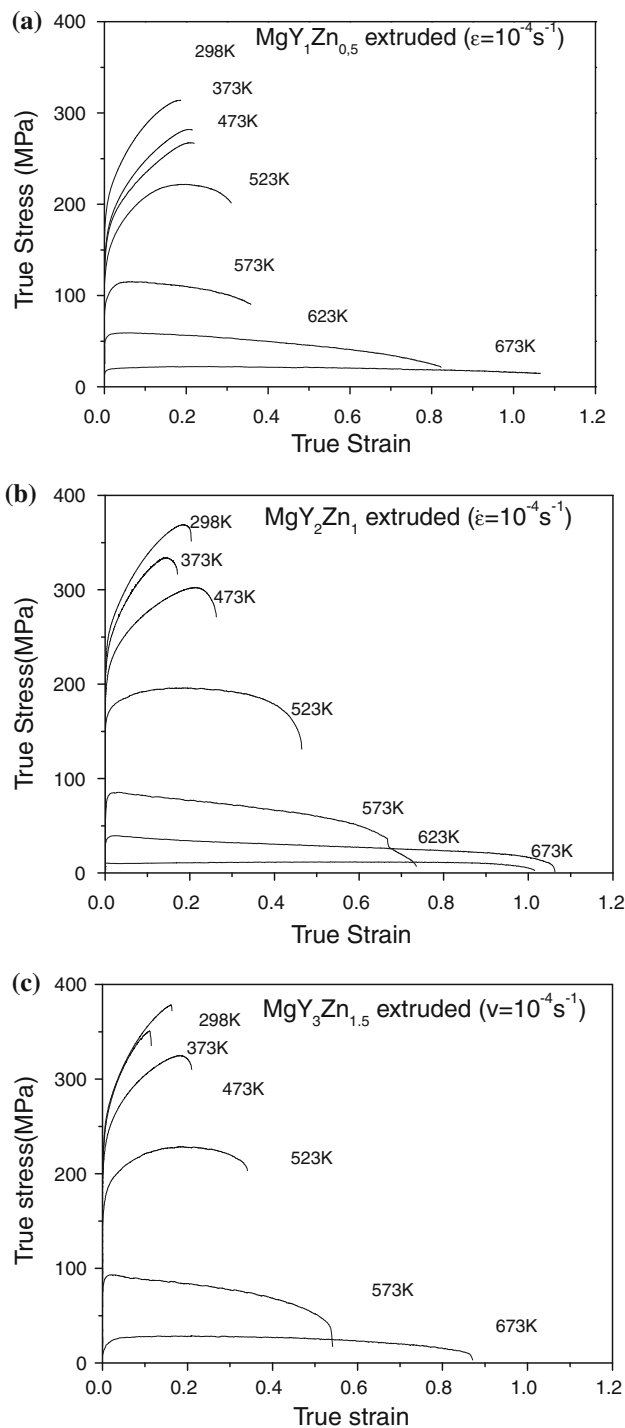


Fig. 10 True stress–true strain curves of extruded alloys from room temperature to 673 K **a** $MgY_1Zn_{0.5}$, **b** MgY_2Zn_1 and **c** $MgY_3Zn_{1.5}$

other hand, Fig. 9b presents a bright field image of the 14H structure. The associated SAED pattern recorded in the $\langle \bar{1}\bar{1}20 \rangle_x$ zone axis and the high magnification image showing a fringe spacing of about 1.8 nm confirm a 14H LPSO structure, not resolved in the XRD patterns. During the extrusion process, the 18R LPSO phase tends to transform into

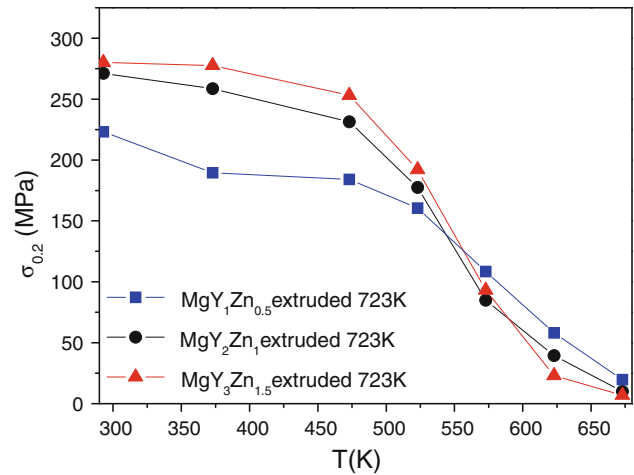


Fig. 11 Yield strength values as a function of test temperature for the three alloys

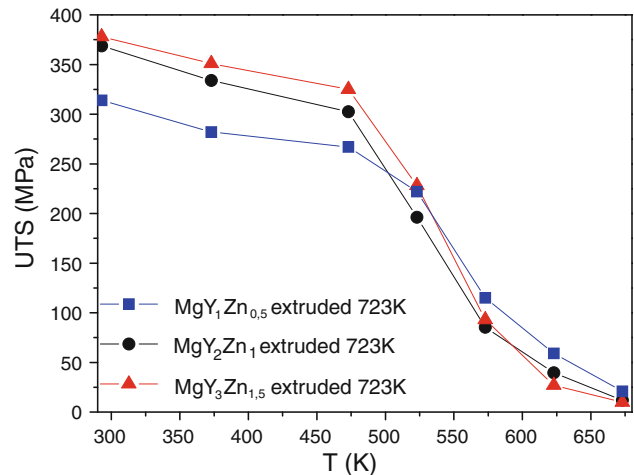


Fig. 12 UTS values as a function of test temperature for the three alloys

a 14H structure. Moreover, the short holding time at the extrusion temperature makes both structures can coexist in the extruded bars.

As mentioned before, isolated plates within the magnesium grains were observed (Fig. 4). These fully coherent long plates have been reported as 14H LPSO structure [13].

Mechanical properties

Hardness results are listed in Table 1. There is a high increase in hardness as the volume fraction of LPSO phase increase. These results demonstrate that LPSO phase has an important reinforcement effect in magnesium. Therefore, this kind of two-phase alloys can be considered as a composite material, where the LPSO phase reinforces the magnesium matrix. This assumption agrees with recent studies [26, 29]. Young’s modulus of both phases has been

evaluated to support this statement. The values for the magnesium matrix and the LPSO phase measured by micro-indentation method are 49.3 ± 1.2 and 102.3 ± 5.5 GPa, respectively.

Figures 10a, c shows the true stress–true strain curves of extruded $\text{MgY}_1\text{Zn}_{0.5}$, MgY_2Zn_1 and $\text{MgY}_3\text{Zn}_{1.5}$ alloys from room temperature to 673 K. In these three materials, a gradual decrease in yield stress and UTS values is observed as temperature increases, although the sharp decrease takes place greater than 523 K. Thus, at 573 K, yield stress values for the three alloys drop to about 100 MPa. From room temperature to 523 K, tensile curves are characterised by significant work hardening. Load transfer from the magnesium matrix to the LPSO phase is expected because the Young's modulus of the LPSO phase is twice that of the magnesium matrix. The elongation at room temperature in the three alloys is always superior to 15% independently of the alloy composition.

Yield strength and UTS values as a function of test temperature for the three alloys are also compared in Figs. 11 and 12. From these figures, it can be followed that the yield stress at room temperature increases with the increase in the volume fraction of the LPSO phase, from 200 MPa for the $\text{MgY}_1\text{Zn}_{0.5}$ to 260 MPa in the case of $\text{MgY}_3\text{Zn}_{1.5}$, which agrees with hardness values. This behaviour remains up to 523 K. Beyond 523 K, the alloy with the lowest volume fraction of the LPSO phase ($\text{MgY}_1\text{Zn}_{0.5}$) exhibits the highest mechanical strength. The coarser-grained alloy ($\text{MgY}_1\text{Zn}_{0.5}$) presents the best strength at high temperatures, indicating that LPSO phase hardening is effective up to 523 K.

This different behaviour at high temperatures should be related to the change in the mechanism controlling the deformation. The high temperature behaviour in metallic materials is normally described by a power law behaviour that represents the relationship between flow stress and strain rate [30]

$$\dot{\epsilon} = A \left(\frac{DGb}{kT} \right) \left(\frac{\sigma}{E} \right)^n, \quad (1)$$

where $\dot{\epsilon}$ is the strain rate, A a constant, σ the applied stress, E the Young's modulus, k the Boltzmann's constant, n the stress exponent, T the absolute temperature and D the diffusion coefficient. For different deformation mechanism such as grain boundary sliding (GBS), there is an important dependence of the strain rate with the grain size. Therefore, a grain size dependence is included in Eq. (1) by:

$$\dot{\epsilon} = A \left(\frac{DGb}{kT} \right) \left(\frac{b}{d} \right)^p \left(\frac{\sigma}{E} \right)^n \quad (2)$$

where d the grain size, b the Burgers vector and p the grain size exponent.

Kawamura et al. [31] has observed stress exponent near $n \sim 2$ in MgY_2Zn_1 alloy with small grains. Moreover, the presence of the LPSO helps to the GBS mechanism. Similar features have been previously reported during the superplastic deformation of multiphase $\text{Mg}_{94}\text{Ni}_3\text{Y}_{1.5}\text{CeMM}_{1.5}$ (%at.) alloy [32]. The microstructure of this alloy consisted on LPSO phase and $\text{Mg}_{17}\text{RE}_2$ particles distributed at grain boundaries of magnesium grains. During deformation, LPSO and intermetallic particles are broken and redistributed within the magnesium matrix. This particle redistribution prevents grain coarsening along the deformation in such a way that GBS mechanism can operate throughout the test. Therefore, it is expected that GBS mechanism takes place in these alloys at high temperature. The high elongation obtained for temperatures higher than 523 K agrees with these assumptions. However, tests at different strain rate are now in process to support this argument.

It is worthy to point out that although the volume fraction of the LPSO phase is higher in the $\text{MgY}_3\text{Zn}_{1.5}$ than in the MgY_2Zn_1 alloy, the hardness and yield stress values are similar. This fact can be because of the morphology of the LPSO phase in the extruded MgY_2Zn_1 alloy (Fig. 2b). It can be supposed that during extrusion, the LPSO phase in MgY_2Zn_1 alloy is easier deformed and oriented in the extrusion direction than in the $\text{MgY}_3\text{Zn}_{1.5}$, becoming a long fiber shape. Therefore, the load transfer mechanism should be more effective than in the case of the $\text{MgY}_3\text{Zn}_{1.5}$ alloy.

Conclusions

The effects of the volume fraction of LPSO phase on microstructure and mechanical properties in three extruded $\text{Mg}_{100-3x}\text{Y}_{2x}\text{Zn}_x$ (%at) alloys have been studied. The following conclusions can be drawn:

1. There is a refinement of the magnesium matrix in the vicinity of the LPSO phase because of new recrystallised grains are nucleated through the PSN mechanism. This effect is more pronounced as the volume fraction of LPSO phase increases.
2. During extrusion process, 18R LPSO structure transforms into the 14H structure. Both structures co-exist in the extruded alloys.
3. The yield stress at room temperature increases with the increase of the volume fraction of LPSO phase. On one hand, the decrease in grain size with the increase in the LPSO volume fraction contributes to the mechanical strength of these alloys because of Hall–Petch effect. On the other hand, the LPSO phase carries an additional load transferred by magnesium grains and,

therefore, these alloys behave as magnesium matrix composites.

- The reinforcing effect of the LPSO phase is important up to 523 K. Above this temperature, the $\text{MgY}_1\text{Zn}_{0.5}$ alloy showed higher mechanical strength because the grain size effect becomes more important.

Acknowledgements This work was supported by the Ministry of Science and Innovation through the MAT2006-11731 Project. E. Oñorbe also thanks the CSIC her JAE contract.

References

- Kainer KU (2000) Magnesium alloys and their applications. Wiley-VCH, Weinheim, Germany
- Pekguleryuz MO, Kaya AA (2003) *Adv Eng Mat* 5(12):866
- Tsai AP, Murakami Y, Niikura A (2000) *Philos Mag Lett* 80:1043
- Lee JY, Kim DH, Lim HK, Kim DH (2005) *Mater Lett* 59:3801
- Luo ZP, Zhang SQ (2000) *J Mater Sci Lett* 19(9):813
- Singh A, Watanabe M, Kato A, Tsai AP (2004) *Scr Mater* 51(10):955
- Inoue A, Kawamura Y, Matsushita M, Hayashi K, Koike J (2001) *J Mater Res* 16:1894
- Abe E, Kawamura Y, Hayashi K, Inoue A (2002) *Acta Mater* 50:3845
- Matsuda M, Li S, Kawamura Y, Ikuhara Y, Nishida M (2005) *Mater Sci Eng A* 393:269
- Chino Y, Mabuchi M, Hagiwara S, Iwasaki H, Yamamoto A, Tsubakino H (2004) *Scr Mater* 51:711
- Nishida M, Kawamura Y, Yamamuro T (2004) *Mater Sci Eng A* 375–377:1217
- Luo ZP, Zhang SQ (2000) *J Mater Sci Lett* 19:813
- Zhu YM, Morton AJ, Nie JF (2010) *Acta Mater* 58:2936
- Kawamura Y, Kasahara T, Izumi S, Yamasaki M (2006) *Scr Mater* 55:453
- Matsuda M, Ando S, Nishida M (2005) *Mater Trans* 46:361
- Datta A, Waghmare UV, Ramamurty U (2008) *Acta Mater* 56:2531
- Matsuda M, Ii S, Kawamura Y, Ikuhara Y, Nishida M (2004) *Mater Sci Eng A* 386:447
- Hagihara K, Yokotani N, Umakoshi Y (2010) *Intermetallics* 18:267
- Shao XH, Yang ZQ, Maa XL (2010) *Acta Mater* 58:4760
- Oliver WC, Pharr GM (1992) *J Mater Res* 7(6):1564
- Ball EA, Prangnell PB (1994) *Scr Metall Mater* 31(2):111
- Robson JD, Henry DT, Davis B (2009) *Acta Mater* 57:2739
- Yamasaki M, Hashimoto K, Hagihara K, Kawamura Y (2011) *Acta Mater* 59(9):3646
- CaRine Crystallography 3.1 Software. Divergent S.A. Centre de Transfert 60200 Compiègne France. <http://carine.crystallography.pagesproorange.fr/>
- Hagihara K, Kinoshita A, Sugino Y, Yamasaki M, Kawamura Y, Yasuda HY, Umakoshi Y (2010) *Acta Mater* 58(19):6282
- Itoi T, Seimiya T, Kawamura Y, Hirohashi M (2004) *Scr Mater* 51(2):107
- Zhu YM, Wayland M, Morton AJ, Oh-ishi K, Hono K, Nie JF (2009) *Scr Mater* 60(11):980
- Yoshimoto S, Yamasaki M, Kawamura Y (2006) *Mater Trans* 47(4):959
- Oñorbe E, Garcés G, Pérez P, Cabeza S, Klaus M, Genzel C, Frutos E, Adeva P (2011) *Scr Mater*. doi:10.1016/j.scriptamat.2011.07.017
- Mishra RS, Bieler TR, Mukherjee AK (1997) *Acta Mater* 45(2):561
- Kawamura Y, Hayashi K, Inoue A, Masumoto T (2001) *Mat Trans* 42:1172
- Pérez P, Eddahbi M, González S, Garcés G, Adeva P (2011) *Scr Mater* 64(1):33